Journal of Theoretical and Applied Mechanics, Sofia, Vol.51 (2021) pp. 437-451
SOLID MECHANICS

THE PLANAR BUCKLING OF PINNED-FIXED SHALLOW ARCHES

LÁSZLÓ PÉTER KISS[1]*, PUSTA JALALOVA[2], ZIYA MEHDIYEV[2]

[1]*Institute of Applied Mechanics, University of Miskolc, 3515 Miskolc-Egyetemváros, Hungary*

[2]*University of Miskolc, 3515 Miskolc-Egyetemváros, Hungary*

[Received: 02 April 2020. Accepted: 20 September 2021

ABSTRACT: The article is devoted to the static, planar buckling problem of pinned-fixed shallow circular arches subject to a concentrated force. The nonlinear model is based on the single-layer Euler-Bernoulli theory. The related coupled differential equations of equilibrium are solved in closed-form. It is found such arches can undergo limit point buckling. The model is applicable not only to homogeneous but also for nonhomogeneous material distributions. The analytical results are compared with the results for pinned-pinned and fixed-fixed members. There are certain geometries and material distributions when the buckling load is almost the same for all these three support arrangements. Otherwise, as the included angle is increased, the difference between the critical loads also increases. The new findings are validated by means of literature and finite element results.

KEY WORDS: buckling, composite materials, snap-through, stiffness, arch.

1 INTRODUCTION

The buckling of various structural members is a well-known phenomenon. The very first pioneering findings in this topic are related to the classical Euler column. As for such straight columns made of classical, homogeneous material, there is still ongoing research with important new finding as recently published in the likes of [1–6, 9–11]. For instance, the authors of [7] focus on the buckling of thin-walled columns. The boundary value problem is solved effectively by the Fourier cosine series method. Meanwhile, in [8], the stability of shear deformable thick beams under transverse and axial loads is investigated by the method of trial function.

Considering homogeneous curved beams (arches), some further articles should be mentioned. The main objective of paper [12] is to find a solution to the problem of equilibrium stability of a plane double-hinged arch under a dead load. The problem is solved considering all of the axial, shear and bending stiffnesses. Comparisons

*Corresponding author e-mail: mechkiss@uni-miskolc.hu

are made between the achieved result and the classical Kornoukhov-Dinnik solution which is based only on bending stiffness. Work [13] analyzes the snap-through of arches and buckled beams. Snap-through of arches and buckled beams are pushed downward from above at a specific location along the span until they jump to a completely inverted shape. For buckled beams, critical displacements are computed with both ends pinned, both ends clamped, or one end clamped and the other end pinned, and curves of this displacement versus the push-down location are presented. Articles like [14–19] investigate the stability of shallow circular arches under various support and load conditions. The single layer Euler-Bernoulli hypothesis is assumed in these nonlinear models. Meanwhile, in [20], not only single but multi-span continuous arches are studied analytically. As for arbitrary radial or vertical point loads, [21–23] should be mentioned.

Since nonhomogeneous materials are gradually getting more and more common, there is a need for research to understand the mechanical behaviour of elements made of these materials. The number of available articles is huge and the topics are really widespread as can be seen in, e.g., [24–31]. Focusing now on curved beams, article [32] analyses functionally graded (FG) porous arches with graphene platelet reinforcements under uniform radial pressure. The nonlinear elastic equations, based on the Euler-Bernoulli hypothesis, are derived by adopting the potential energy method. Contribution [33] investigates the nonlinear in-plane equilibrium path and buckling behavior of laminated circular shallow arches. The investigations are based on the classical laminate theory. Analytical solutions are validated against the results of finite element simulation and experiments in which the effects of the ply angle and thickness of the laminates and the rise-span ratio of the arch to the critical bucking load and the nonlinear balance path of the laminated arches are all assessed. In [34] the Rayleigh-Ritz method is used to study the large deflection behavior of the small, symmetrically laminated, shallow circular arches subjected to central concentrated load. The symmetric deformation path is studied, and a detailed analysis is conducted at the bifurcation point, onto an asymmetric deformation path for a pinned symmetrically laminated shallow arch. Paper [35] investigates composite curved beams with a geometrically nonlinear finite element model that can analyze moderately large rotations of the cross-sections, the buckling and post-buckling behaviors of composite curved beams with specific elastic reactions in tension and compression. Furthermore, [36] aims to investigate the in-plane buckling behavior of fixed orthotropic composite shallow arches under arbitrary radial point load by means of a combined theoretical, computational and experimental study. The aim of [37] is to investigate the effect of various parameters on bending, buckling and free vibration behaviors of functionally graded curved beams with variable curvatures by using isometric analysis. Paper [38] focuses on the thermoelastic behavior and thermoe-

lastic lateral-torsional buckling of circular arches having in-plane elastic-rotationally restrained ends under an arbitrary radial point load in a uniform thermal environment accounting for shear deformations. The theoretical solutions for the thermoelastic lateral-torsional buckling are derived and the effects of the critical load, the elastic rotational restraints, and temperature field for the elastic buckling of arches accounting for shear deformations are explored. Paper [39] targets to analyze the in-plane instability of fixed arches underneath a linear temperature gradient area and a uniformly dispensed radial load by the use of the effective centroid approach and virtual work principle, while [40] introduces a two-step perturbation technique to model FGM shallow arches on elastic foundation.

Overall, it turns out that the majority of the articles assume identical end-supports when tackling the buckling behaviour of arches. However, in real structures, arches often have different end-constraints. So the behaviour of such members should also be addressed. The current article intends to focus on the in-plane buckling of non-homogeneous pinned-fixed shallow arches under a vertical load at the crown point. The equilibrium equations are given and solved in closed-form. An analytical model is presented to find the nonlinear load-strain relationship and the limit points on the equilibrium path in terms of the geometry and material distribution. Results are also given for pinned-pinned and fixed-fixed members for comparative purposes. Solutions are compared and validated with other literature results and finite element computations.

2 Problem Formulation & Equilibrium Equations

An arch with included angle 2ϑ is constrained by pin at one end and is clamped at the other foundation so that out-of-plane movements are restricted. The centroidal axis is of constant initial curvature ρ. The local base is defined by the axial coordinate $\xi = s$, normal coordinate ζ while η is perpendicular to the plane of the curved member. The loading is a concentrated vertical force at the crown point ($\varphi = 0$).

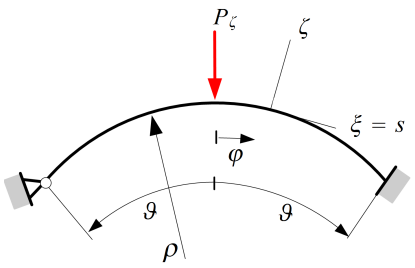

Fig. 1: The centroidal axis of a pinned-fixed arch under external load.

With the Euler-Bernoulli hypothesis [14], the nonlinear membrane strain is given by

$$\varepsilon_m = \frac{\mathrm{d}u_o}{\mathrm{d}s} + \frac{w_o}{\rho} + \frac{1}{2}\psi_{o\eta}^2 \tag{1}$$

with the later term being the rigid body rotation about η:

$$\psi_{o\eta} = \frac{u_o}{\rho} - \frac{\mathrm{d}w_o}{\mathrm{d}s}. \tag{2}$$

Here, u_o and w_o are the tangential and normal displacement components. Moreover, the axial force and bending moment [41] are given by

$$N = A_e\varepsilon_m - \frac{I_{e\eta}}{\rho}\frac{\mathrm{d}\psi_{o\eta}}{\mathrm{d}s}, \tag{3a}$$

$$M = -I_{e\eta}\left(\frac{\mathrm{d}^2 w_o}{\mathrm{d}s^2} + \frac{w_o}{\rho^2}\right), \tag{3b}$$

where geometrical-material properties A_e and $I_{e\eta}$ are defined by

$$A_e = \int_A E\mathrm{d}A, \qquad I_{e\eta} = \int_A \zeta^2 E\mathrm{d}A. \tag{4}$$

Thus, the model can tackle not only homogeneous but heterogeneous or inhomogeneous material distributions as long as the material is linearly elastic and isotropic. E denotes the modulus of elasticity – it can be a function of the cross-sectional coordinates $\eta;\zeta$ given that $E(\eta;\zeta) = E(-\eta;\zeta)$ is satisfied.

Derivatives taken with respect to the arc coordinate s and the angle coordinate φ relate to each other. The derivatives of these are noted briefly by

$$\frac{\mathrm{d}^n(\ldots)}{\mathrm{d}s^n} = \frac{1}{\rho^n}\frac{\mathrm{d}^n(\ldots)}{\mathrm{d}\varphi^n} = (\ldots)^{(n)}, \quad n \in \mathbb{Z}. \tag{5}$$

Furthermore, dimensionless displacements $W_o = w_o/\rho$; $U_o = u_o/\rho$ will also be introduced in the proceeding.

Writing the principle of virtual work for the system – as detailed in [41] – yields the coupled static equilibrium equations

$$\begin{aligned} &\frac{\mathrm{d}N}{\mathrm{d}s} + \frac{1}{\rho}\left[\frac{\mathrm{d}M}{\mathrm{d}s} - \left(N + \frac{M}{\rho}\right)\psi_{o\eta}\right] = 0\,, \\ &\frac{\mathrm{d}}{\mathrm{d}s}\left[\frac{\mathrm{d}M}{\mathrm{d}s} - \left(N + \frac{M}{\rho}\right)\psi_{o\eta}\right] - \frac{N}{\rho} = 0\,, \end{aligned} \tag{6}$$

meanwhile, the related boundary conditions for pinned-fixed arches are

$$W_o|_{\pm\vartheta} = \psi_{o\eta}|_{\vartheta} = M|_{-\vartheta} = 0. \tag{7}$$

These previous conditions can be given in terms of the displacements using Eqs. (2)-(4). While the displacements, rotation and bending moment are continuous in φ throughout the arch, the shear force distribution has a discontinuity of P_ζ at the application point of the external force:

$$\left[\frac{\mathrm{d}M}{\mathrm{d}s} - \left(N + \frac{M}{\rho}\right)\psi_{o\eta}\right]\Bigg|_{\varphi=+0} - \left[\frac{\mathrm{d}M}{\mathrm{d}s} - \left(N + \frac{M}{\rho}\right)\psi_{o\eta}\right]\Bigg|_{\varphi=-0} = P_\zeta. \tag{8}$$

Plugging basic relations (1)-(4) to (6) yields [43]

$$\varepsilon_m^{(1)} = 0 \tag{9}$$

and

$$W_o^{(4)} + \left(\chi^2 + 1\right) W_o^{(2)} + \chi^2 W_o = \chi^2 - 1 \tag{10}$$

with

$$m = A_e\rho^2/I_{e\eta}; \qquad \chi^2 = 1 - m\varepsilon_m. \tag{11}$$

These above axial and radial equilibrium equations must, therefore, be satisfied. It is noted that parameter m contains the effect of the material distribution and the geometry.

3 Solution Algorithm

There exists closed-form solution to Eq. (10), that is

$$W_o(\varphi = -\vartheta ... 0) = \frac{\chi^2 - 1}{\chi^2} + A_1\cos\varphi + A_2\sin\varphi - \frac{A_3}{\chi^2}\cos\chi\varphi - \frac{A_4}{\chi^2}\sin\chi\varphi, \tag{12a}$$

$$W_o(\varphi = 0 ... \vartheta) = \frac{\chi^2 - 1}{\chi^2} + B_1\cos\varphi + B_2\sin\varphi - \frac{B_3}{\chi^2}\cos\chi\varphi - \frac{B_4}{\chi^2}\sin\chi\varphi. \tag{12b}$$

The constants $A_i; B_i$ can be found by recalling boundary and discontinuity conditions (7)-(8). The coefficients are listed hereinafter:

$$A_1 = B_1 = \frac{-1}{\chi^2\vartheta\left(\chi^2-1\right)\sin\chi\vartheta\cos\chi\vartheta\cos\vartheta\sin\vartheta\left(1-2\cos^2\vartheta\right)\left(2\cos^2\chi\vartheta-1\right)}$$
$$\times\Big[\vartheta\left(\chi^2-1\right)\left(\left(2\chi^2\cos^2\chi\vartheta - \chi^2 + \sin^2\chi\vartheta\right)\sin\vartheta - \chi\cos\chi\vartheta\sin\chi\vartheta\cos\vartheta\right)$$
$$- \mathcal{P}\chi\sin\vartheta\left(2\chi\sin\vartheta\cos^2\chi\vartheta - \chi\sin\vartheta + \sin\chi\vartheta - 2\sin\chi\vartheta\cos\chi\vartheta\cos\vartheta\right)\Big]$$

$$A_2 = -C^{-1} \times \left[\vartheta\left(\chi^2-1\right)\sin\chi\vartheta\left(\chi\cos\chi\vartheta\sin\vartheta-\cos\vartheta\sin\chi\vartheta\right)-\mathcal{P}\chi\left(2\cos\chi\vartheta\cos\vartheta\right.\right.$$
$$\left.\left.\times\left(\chi\cos\chi\vartheta\sin\vartheta-\cos\vartheta\sin\chi\vartheta\right)-\cos\vartheta\left(\chi\sin\vartheta+\sin\chi\vartheta\right)+2\sin\chi\vartheta\cos\chi\vartheta\right]\right.$$

$$B_2 = -C^{-1} \times \left[\vartheta\left(\chi^2-1\right)\sin\chi\vartheta\left(\chi\cos\chi\vartheta\sin\vartheta-\cos\vartheta\sin\chi\vartheta\right)\right.$$
$$\left.+\,\mathcal{P}\chi\left(\cos\vartheta\right)\left(+2\chi\sin\vartheta\cos^2\chi\vartheta-\chi\sin\vartheta+\sin\chi\vartheta-2\sin\chi\vartheta\cos\chi\vartheta\cos\vartheta\right)\right]$$

$$C = \left(\chi^2-1\right)$$
$$\times\,\vartheta\chi\left(\sin\chi\vartheta\cos\chi\vartheta-2\sin\chi\vartheta\cos\chi\vartheta\cos^2\vartheta-\chi\cos\vartheta\sin\vartheta+2\chi\cos\vartheta\sin\vartheta\cos^2\chi\vartheta\right)$$

$$A_3 = B_3 = \left[\chi\mathcal{P}\sin\chi\vartheta\left(-\chi\sin\vartheta-2\sin\chi\vartheta\cos^2\vartheta+\sin\chi\vartheta+2\chi\cos\chi\vartheta\cos\vartheta\sin\vartheta\right)\right.$$
$$\left.-\,\vartheta\left(\chi^2-1\right)\left(\chi\cos\chi\vartheta\cos\vartheta\sin\vartheta-\sin\chi\vartheta\left(\chi^2\sin^2\vartheta+\cos^2\vartheta-\sin^2\vartheta\right)\right)\right]$$
$$\times\left[\left(\sin\chi\vartheta\cos\chi\vartheta-2\sin\chi\vartheta\cos\chi\vartheta\cos^2\vartheta-\chi\cos\vartheta\sin\vartheta+2\chi\cos\vartheta\sin\vartheta\cos^2\chi\vartheta\right)\left(\chi^2-1\right)\vartheta\right]^{-1}$$

$$A_4 = -\frac{\chi}{D}\left[\vartheta\sin\vartheta\left(\chi^2-1\right)\left(-\cos\vartheta\sin\chi\vartheta+\chi\cos\chi\vartheta\sin\vartheta\right)\right.$$
$$-\,\mathcal{P}\left(\sin\chi\vartheta\cos\chi\vartheta\sin^2\vartheta-\sin\chi\vartheta\cos\chi\vartheta\cos^2\vartheta\right.$$
$$\left.\left.-2\chi\cos\vartheta\sin\vartheta\sin^2\chi\vartheta+\chi\cos\chi\vartheta\cos^2\vartheta\sin\vartheta+\chi\cos\chi\vartheta\sin^3\vartheta\right)\right]$$

$$B_4 = -\frac{\chi}{D}\left[\vartheta\sin\vartheta\left(\chi^2-1\right)\left(-\cos\vartheta\sin\chi\vartheta+\chi\cos\chi\vartheta\sin\vartheta\right)+\mathcal{P}\cos\chi\vartheta\right.$$
$$\left.\times\,\left(2\chi\cos\chi\vartheta\cos\vartheta\sin\vartheta-\chi\cos^2\vartheta\sin\vartheta-\sin\chi\vartheta\cos^2\vartheta-\chi\sin^3\vartheta+\sin^2\vartheta\sin\chi\vartheta\right)\right]$$

$$D = \left(\chi^2-1\right)\vartheta$$
$$\times\left[\cos\vartheta\left(-2\sin\chi\vartheta\cos\chi\vartheta\cos\vartheta-\chi\sin\vartheta+2\chi\sin\vartheta\cos^2\chi\vartheta\right)+\sin\chi\vartheta\cos\chi\vartheta\right].$$

In these equations $\mathcal{P}$ is introduced as the dimensionless load

$$\mathcal{P} = \frac{-P_\zeta\rho^2\vartheta}{2I_{e\eta}}. \tag{13}$$

According to the equilibrium equations, as the membrane strain is constant (9), substituting solutions (12a)-(12b) into (1) and taking its average over the whole arch yields a nonlinear relationship between the strain parameter χ and the dimensionless load $\mathcal{P}$ as

$$\varepsilon_m = \frac{1}{2\vartheta}\int_{-\vartheta}^{\vartheta} \varepsilon_m \mathrm{d}\varphi \simeq \frac{1}{2\vartheta}\int_{-\vartheta}^{\vartheta}\left(U_o^{(1)} + W_o + \frac{1}{2}W_o^{(1)}W_o^{(1)}\right)\mathrm{d}\varphi = C_1\mathcal{P}^2 + C_2\mathcal{P} + C_3. \tag{14}$$

The $C_i;\ i = 1, 2, 3$ constants in this formula can be calculated in closed-form. Since this relation must hold for any geometry and material distribution and strain parameter, it is possible to find the load-strain relationship. Thus, the critical strains and loads for limit point buckling can as well be found. Because pinned-fixed shallow circular arches cannot undergo bifurcation buckling [15], the limit point (or snap-through) phenomenon should be addressed in details.

4 Results & Discussion

Analytical evaluation of the model is presented hereinafter. Results found for pinned-fixed (p-f) supports are compared to pinned-pinned (p-p) and fixed-fixed (f-f) findings of [41–43] to reveal the differences. The main objective is to find the lowest critical (buckling) loads. During our efforts, the quotient of the arch length $S = 2\rho\vartheta$ and the E-weighted radius of gyration $r = \sqrt{I_{e\eta}/A_e}$ is selected to have three typical values: $75, 100$ and 150. Comparisons will be given with other literature models and finite element computations for validation purposes.

In Figs. 2-4, the buckling loads are plotted against the semi-vertex angle for three S/r ratios. A notable difference between the supports is that, while pinned-fixed and fixed-fixed members might lose their stability in a limit point mode only, for pinned-pinned arches, first, there is limit point buckling but with the angle increasing, it is preceded by bifurcation buckling [41, 42]. Clearly, the load-bearing capabilities are best for fixed-fixed members and least favourable for pinned-pinned ones throughout.

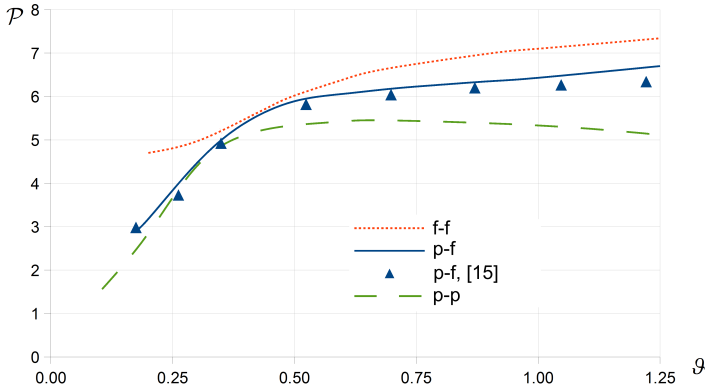

Fig. 2: Lowest buckling loads for three support arrangements, $S/r = 75$.

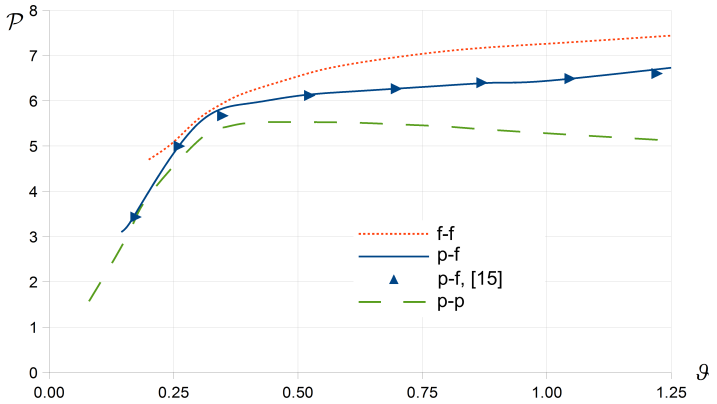

Fig. 3: Lowest buckling loads for three support arrangements, $S/r = 100$.

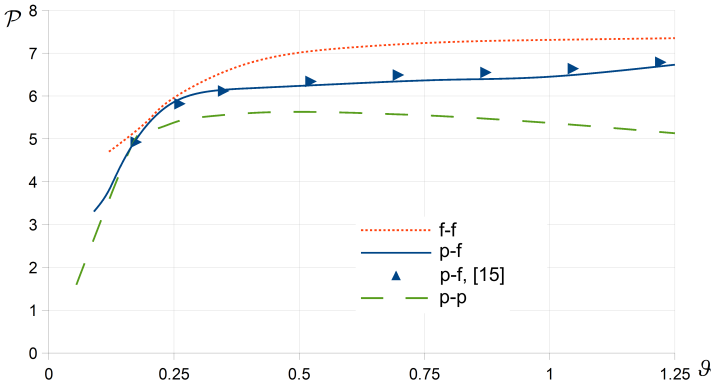

Fig. 4: Lowest buckling loads for three support arrangements, $S/r = 150$.

However, there is always a small range in ϑ, where the critical loads are so close – it is around $0.2...0.4$ in the related figures, depending on S/r. Meanwhile the buckling loads tend to gradually increase for fixed-fixed and pinned-fixed structural elements, for pinned-pinned arches, after a while, it starts to descend slowly, making the greatest relative difference up to 48% at $\vartheta = 1.25$ between p-p and f-f supports. Increasing S/r shifts the typical curves to the left. Figures 2-4 also contain the solutions of [15] as markers for pinned-fixed case.

When plotting and comparing the pinned-fixed results for the different cases – Fig. 5 – it is clear that arches with the highest S/r ratio bear the greatest loads initially but the solutions tend to the same limit as the angle is increased. It can be said that as of $\vartheta \simeq 0.7$ the critical loads become independent of S/r.

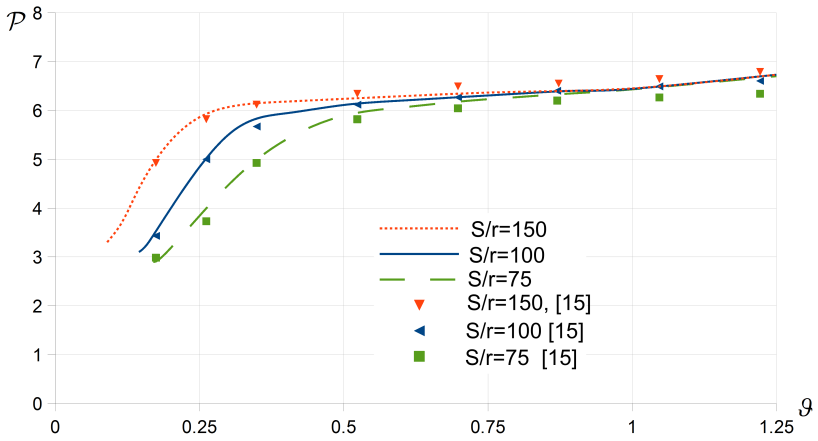

Fig. 5: Lowest buckling loads of pinned-fixed members for three S/r ratios.

Figure 6 shows the dimensionless radial displacement of the loading point ($W_{oC} = W_o(\varphi = 0)$) against the dimensionless load $\mathcal{P}$. The typical in-plane behaviour – equilibrium paths – are drawn for $S/r = 100$ and $\vartheta = 0.3$ to demonstrate how different these can be just because of the support change. Figure part (a) is for fixed-fixed, (b) is for pinned-fixed and (c) is for pinned-pinned constraints. In Fig. 6a, there are three equilibrium branches: one primary stable, one remote stable and one unstable

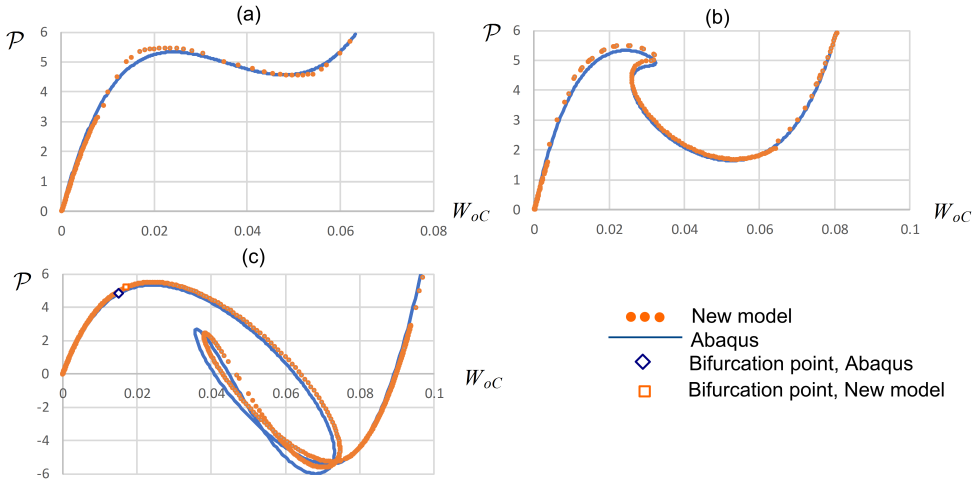

Fig. 6: The in-plane behaviour of (a) f-f, (b) p-f, (c) p-p arches when $\vartheta = 0.3$ and S/r=100

between these two. Further, it contains two limit points. When increasing the load gradually, just above the value of the first limit point, there is no adjacent equilibrium configuration but only a distinct one, so, with a sudden increase in the displacement, the arch snaps-through to this new state. After that, a gradual increase in the load yields gradual increase in the displacement. Part (b) is plotted for pinned-fixed supports, and meanwhile, it contains, again, two stable branches, the number of unstable ones is now three. However, in figure part (c), there are four unstable branches with four limit points. But there is a bifurcation point before the first upper limit point so, when reaching that, the arch buckles to an infinitesimally close equilibrium state [14].

These three figure parts show that not only the lowest buckling load but also the lowest (dimensionless) displacement is related to pinned-pinned supports, while fixed-fixed members hold the greatest ones of these values. In Figs. 6, the new model is compared with the calculations of the commercial finite element software Abaqus 6.13. A one-dimensional $B21$ element was used for the mapping. The number of elements was 80 and it proved enough to achieve converged results. The Static/Risk step was selected to track the equilibrium paths. The cross-section was a uniform doubly symmetric I-shape with a typical depth of 256 mm, flange width of 146 mm, flange thickness of 10.9 mm and web thickness of 6 mm. Geometric imperfections were also introduced for the pinned-pinned case to find the bifurcation point numerically. The correlation is really good between the models, not only in the buckling load but also in the equilibrium paths.

Next, in Fig. 7, the changes in the equilibrium path can be seen as ϑ is set to $0.3; 0.6$ and 0.9. In accord with Figs. 2-4, the buckling load gradually increases with the angle. Furthermore, there is no change in the number of equilibrium branches – two stable and three unstable ones are found. Surely, the displacement corresponding to the first upper limit point also shows an increase. Again, the Abaqus model confirms the validity of our findings. Finally, some further comparisons are shown in Table 1.

Table 1: Validation of the results using Abaqus for $S/r = 100$

supports	ϑ	$\mathcal{P}$	$\mathcal{P}_{\text{Abaqus}}$
f-f /p-f / p-p	0.3	$5.62/5.50/5.12$	$5.34/5.32/4.99$
f-f /p-f / p-p	0.6	$6.80/6.22/5.52$	$6.48/6.12/5.38$
f-f /p-f / p-p	0.9	$7.18/6.41/5.35$	$6.90/6.43/5.27$

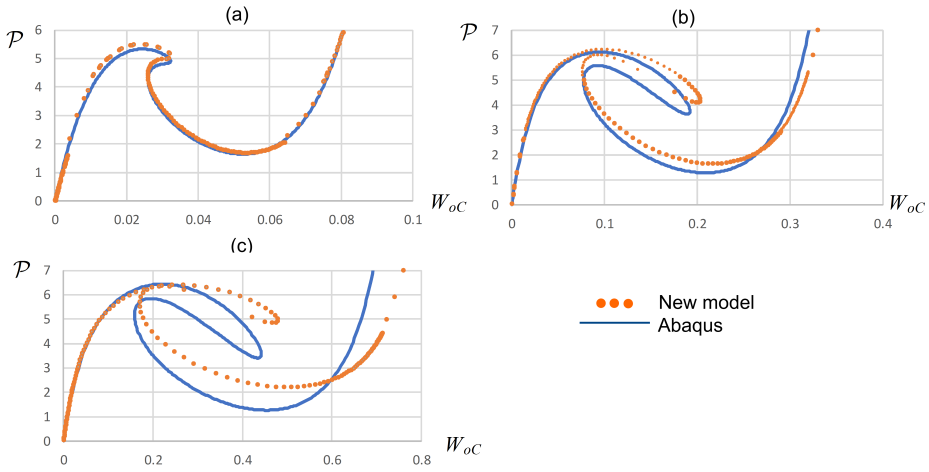

Fig. 7: In-plane behaviour of p-f arches when ϑ is (a) 0.3; (b) 0.6; (c) 0.9 and $S/r = 100$.

5 Conclusions

The article tackles the stability and in-plane behaviour of pinned-fixed shallow circular arches. The problem is physically linear and geometrically nonlinear. The one-dimensional beam model is based on the Euler-Bernoulli hypothesis. The related coupled static equilibrium equations are derived using a variational principle. Closed-form analytical solutions are given. The buckling equations are also presented and evaluated. Pinned-fixed members might buckle in a limit point mode only. Parametric studies show that the lowest buckling load for pinned-fixed members is always between the values valid for pinned-pinned and fixed-fixed supports. Despite the different supports, for certain parameter sets, the critical loads are close to each other. The buckling load gradually and continuously increases together with the arch angle for pinned-fixed members. As of $\vartheta \simeq 0.7$ the buckling load becomes independent of the S/r ratio. Some typical equilibrium paths are also shown. For the selected geometries, the number of stabile equilibrium branches is always two, while the number of unstable branches is three. In this respect, this behaviour is also different from pinned-pinned or fixed-fixed members. Comparative studies of the new model with the literature and finite element computations prove the correctness.

Acknowledgements

The described article was carried out as part of the EFOP-3.6.1-16-2016-00011 Younger and Renewing University Innovative Knowledge City institutional development of

the University of Miskolc aiming at intelligent specialisation project implemented in the framework of the Szechenyi 2020 program. The realization of this project is supported by the European Union, co-financed by the European Social Fund.

References

[1] K. Murawski (2018) "Technical Stability of Continuously Loaded Thin-walled Slender Columns.". Lulu Press, Inc.

[2] K. Murawski (2020) Lateral Buckling in Elastic-plastic States of Thin-walled Semi-slender Columns Made of Steel R35 According to Known Hypotheses. pp. 47. DOI: https://doi.org/10.13140/RG.2.2.23578.59845.

[3] K. Murawski (2019) Stability, shell stress and strain technical analysis in elastic states of very slender rectangular column compressed by ball-and-socket joints without friction. pp. 19. DOI: https://doi.org/10.13140/RG.2.2.28299.64808.

[4] O.A. Oguaghamba, C.C. Ike, E. U. Ikwueze, I.O. Ofondu (2019) Finite fourier sine integral transform method for the elastic buckling analysis of doubly-symmetric thin- walled beams with Dirichlet boundary conditions. *ARPN Journal of Engineering and Applied Sciences* **14** (23) 3968–3974.

[5] C.C. Ike, C.U. Nwoji, H.N. Onah, B.O. Mama, M.E. Onyia (2019) Modified Single Finite Fourier Cosine Integral Transform Method for Finding the Critical Elastic Buckling Loads of First Order Shear Deformable Beams with Fixed Ends. *Revue des Composites et des Matériaux Avancés* **29** (6) 357–362. DOI: https://doi.org/10.18280/rcma.290603.

[6] C.C. Ike, C.U. Nwoji, B.O. Mama, H.N. Onah, M.E. Onyia (2019) Laplace Transform Method for the Elastic Buckling Analysis of Moderately Thick Beams. *International Journal of Engineering Research and Technology* **12** (10) 1626–1638.

[7] C.C. Ike, H.N. Onah, B.O. Mama, C.U. Nwoji, E.U. Ikwueze (2019) Fourier Cosine Series Method for Solving the Generalized Elastic Thin-walled Column Buckling Problem for Dirichlet Boundary Conditions. *Revue des Composites et des Materiaux Avances* **29** (3) 131–137. DOI: https://doi.org/10.18280/rcma.290301.

[8] H.N. Onah, C.U. Nwoji, M.E. Onyia, B.O. Mama, C.C. Ike (2020) Exact Solutions for the Elastic Buckling Problem of Moderately Thick Beams. *Revue des Composites et des Materiaux Avances* **30** (2) 83–93. DOI: https://doi.org/10.18280/rcma.300205.

[9] T.V. Nazmeeva, N.I. Vatin (2016) Numerical Investigations of Notched C-Profile Compressed Members with Initial Imperfections. *Magazine of Civil Engineering* **62** (2) 92–101. DOI: https://doi.org/10.5862/MCE.62.9.

[10] M.A. Ali, M. Tomko, M. Badak (2013) Analysis of the resistance of thin-walled cold-formed compressed steel members with closed cross-sections. Part 1. *Magazine of Civil Engineering* **40** (5) 38–45. DOI: https://doi.org/10.5862/MCE.40.4.

[11] A. Javidinejad (2012) Buckling of Beams and Columns under Combined Axial and Horizontal Loading with Various Axial Loading Application Locations. *Journal of Theoretical and Applied Mechanics, Sofia* **42** (2) 19–30.

[12] V. Lalin, A. Dmitriev, S. Diakov (2019) Nonlinear deformation and stability of geometrically exact elastic arches. *Magazine of Civil Engineering* **89** (4) 39–51. DOI: https://doi.org/10.18720/MCE.89.4.

[13] R.H. Plaut (2015) Snap-through of arches and buckled beams under unilateral displacement control. *International Journal of Solids and Structures* **63** 109–113. DOI: https://doi.org/10.1016/j.ijsolstr.2015.02.044.

[14] M.A. Bradford, B. Uy and Y.-L. Pi (2002) In-plane elastic stability of arches under a central concentrated load. *Journal of Engineering Mechanics* **128** (7) 710–719. DOI: https://doi.org/10.1061/(ASCE)0733-9399(2002)128:7(710).

[15] Y.-L. Pi, M.A. Bradford (2012) Non-linear in-plane analysis and buckling of pinned-fixed shallow arches subjected to a central concentrated load. *International Journal of Non-Linear Mechanics* **47** 118–131. DOI: https://doi.org/10.1016/j.ijnonlinmec.2012.04.006.

[16] Y.-L. Pi, M.A. Bradford (2012) Non-linear buckling and postbuckling analysis of arches with unequal rotational end restraints under a central concentrated load. *International Journal of Solids and Structures* **49** 3762–3773. DOI: https://doi.org/10.1016/j.ijsolstr.2012.08.012.

[17] S.-t. Yan, X. Shen, Z. Jin (2018) Instability of imperfect non-uniform shallow arch under uniform radial pressure for pinned and fixed boundary conditions. *Thin-Walled Structures* **132** 217–236. DOI: https://doi.org/10.1016/j.tws.2018.08.018.

[18] S.-t. Yan, X. Shen, Z. Chen, Z. Jin (2017) On buckling of non-uniform shallow arch under a central concentrated load. *International Journal of Mechanical Sciences* **133** 330–343. DOI: https://doi.org/10.1016/j.ijmecsci.2017.08.046.

[19] S.-t. Yan, X. Shen, Z. Chen, Z. Jin (2018) Collapse behavior of non-uniform shallow arch under a concentrated load for fixed and pinned boundary conditions. *International Journal of Mechanical Sciences* **137** 46–67. DOI: https://doi.org/10.1016/j.ijmecsci.2018.01.005.

[20] C.-F. Hu, Y.-M. Huang (2019) In-plane nonlinear elastic stability of pin-ended parabolic multi-span continuous arches. *Engineering Structures* **190** 435–446. DOI: https://doi.org/10.1016/j.engstruct.2019.04.013.

[21] Y.-L. Pi (2006) Non-linear in-plane multiple equilibria and buckling of pin-ended shallow circular arches under an arbitrary radial point load. *Applied Mathematical Modelling* **77** 115–136. DOI: https://doi.org/10.1016/j.apm.2019.07.021.

[22] Y.-L. Pi, M.A. Bradford (2017) Nonlinear Equilibrium and Buckling of Fixed Shallow Arches Subjected to an Arbitrary Radial Concentrated Load. *International Journal of Structural Stability and Dynamics* **17** (8) 1–17. DOI: https://doi.org/10.1142/S0219455417500821.

[23] L.P. Kiss (2020) Stability of fixed-fixed shallow arches under arbitrary radial and vertical forces. *Magazine of Civil Engineering* **95** (3) (In the press.)

[24] D. Gönczi (2018) Analysis of Rotating Functionally Graded Disks with Arbitrary Material Properties. *Acta Technica Corviniensis Bulletin of Engineering* **4** 1–6.

[25] N.D. Duc, P.H. Cong, N.D. Tuan, P. Tran, N.V. Thanh (2017) Thermal and mechanical stability of functionally graded carbon nanotubes (FG CNT)-reinforced composite truncated conical shells surrounded by the elastic foundations. *Thin-Walled Structures* **115** 300–310. DOI: https://doi.org/10.1016/j.tws.2017.02.016.

[26] H. Mashhadban, S.S. Kutanaei, M.A. Sayarinejad (2016) Prediction and modeling of mechanical properties in fiber reinforced self-compacting concrete using particle swarm optimization algorithm and artificial neural network. *Construction and Building Materials* **119** 277–287.
DOI: https://doi.org/10.1016/j.conbuildmat.2016.05.034.

[27] T. Yu, S. Yin, T.Q. Bui, S. Xia, S. Tanaka, S. Hirose (2015) NURBS-based isogeometric analysis of buckling and free vibration problems for laminated composites plates with complicated cutouts using a new simple FSDT theory and level set method. *Thin-Walled Structures* **101** 141–156. DOI: https://doi.org/10.1016/j.tws.2015.12.008.

[28] D. Gönczi, I. Ecsedi (2015) Thermoelastic stresses in nonhomogeneous prismatic bars. *Annals of Faculty of Engineering Hunedoara - International Journal of Engineering* **13** (2) 49–52.

[29] D. Gönczi (2016) Thermal stresses in thin anisotropic hollow circular disk. *Annals of Faculty of Engineering Hunedoara - International Journal of Engineering* **14** (2) 59–64.

[30] P. Angelova (2019) Mechanical and thermal properties of pla based nanocomposites with graphene and carbon nanotubes. *Journal of Theoretical and Applied Mechanics, Sofia* **49** (3) 241–256.

[31] Y. Stoynov, P. Dineva, T. Rangelov (2019) Wave scattering and stress concentration in a magneto-electro-elastic plane with a nano-crack by boundary integral equations. *Journal of Theoretical and Applied Mechanics, Sofia* **49** (3) 203–223.

[32] Z. Liu, C. Yang, W. Gao, D. Wu, G. Li (2019) Nonlinear behaviour and stability of functionally graded porous arches with graphene platelets reinforcements. *International Journal of Engineering Science* **137** 37–56.
DOI: https://doi.org/10.1016/j.ijengsci.2018.12.003.

[33] Z. Zhang, A. Liu, J. Yang, Y. Huang (2019) Nonlinear in-plane elastic buckling of a laminated circular shallow arch subjected to a central concentrated load. *International Journal of Mechanical Sciences* **161-162.**
DOI: https://doi.org/10.1016/j.ijmecsci.2019.105023.

[34] D. Kim, R.A. Chaudhuri (2009) Postbuckling behavior of symmetrically laminated thin shallow circular arches. *Composite Structures* **87** (1) 101–108.
DOI: https://doi.org/10.1016/j.compstruct.2008.01.005.

[35] F. Fraternali, S. Spadea, L. Ascione (2013) Buckling behavior of curved composite beams with different elastic response in tension and compression. *Composite Structures* **100** 280–289. DOI: https://doi.org/10.1016/j.compstruct.2012.12.021.

[36] Z. Zhang, A. Liu, J. Yang, Y.-L. Pi, Y. Huang, J. Fu (2020) A theoretical and experimental study on in-plane buckling of orthotropic composite arches under an arbitrary radial point load. *Composite Structures* **237** Article no. 111933.
DOI: https://doi.org/10.1016/j.compstruct.2020.111933.

[37] T.-A. HUYNH, A.-T. LUU, J. LEE (2017) Bending, buckling and free vibration analyses of functionally graded curved beams with variable curvatures using isogeometric approach. *Meccanica* **52** 2527–2546. DOI: https://doi.org/10.1007/s11012-016-0603-z.

[38] H. LU, A. LIU, Y.-L. PI, M.A. BRADFORD, J. FU (2019) Lateral-torsional buckling of arches under an arbitrary radial point load in a thermal environment incorporating shear deformations. *Engineering Structures* **179** 189–203.
DOI: https://doi.org/10.1016/j.engstruct.2018.10.071.

[39] X. SONG, H. LU, A. LIU, Y. HUANG (2019) In-Plane Instability of Fixed Arches under Linear Temperature Gradient Field and Uniformly Distributed Radial Load. *Mathematical Problems in Engineering* Article ID 5938030.
DOI: https://doi.org/10.1155/2019/5938030.

[40] H. BABAEI, Y. KIANI, M.R. ESLAMI (2018) Thermomechanical nonlinear in-plane analysis of fix-ended FGM shallow arches on nonlinear elastic foundation using two-step perturbation technique. *International Journal of Mechanics and Materials in Design* **15** 225–244. DOI: https://doi.org/10.1007/s10999-018-9420-y.

[41] L. KISS, GY. SZEIDL (2015) Nonlinear In-Plane Stability of Heterogeneous Curved Beams under a Concentrated Radial Load at the Crown Point. *Technische Mechanik* **35** (1) 1–30.

[42] L. KISS, GY. SZEIDL (2015) In-Plane Stability of Fixed-fixed Heterogeneous Curved Beams under a Concentrated Radial Load at the Crown Point. *Technische Mechanik* **35** (1) 31–48.

[43] L.P. KISS (2020) Nonlinear stability analysis of FGM shallow arches under an arbitrary concentrated radial force. *International Journal of Mechanics and Materials in Design* **16** 91–108. DOI: https://doi.org/10.1007/s10999-019-09460-2.